CHAPTER-3

PHYSICAL MICROSTRUCTURAL AND MECHANICAL PROPERTIES EVALUATION

3.1 Introduction

This chapter deals with the evaluation of physical, microstructural and mechanical properties of *insitu* formed AA5052/ZrB_2 composites having different compositions (i.e. 0, 3, 6, 9 and 10 vol. % of ZrB_2 particles). The reaction temperature and formation of ZrB_2 particles were confirmed by DTA and XRD techniques. Physical properties like density and porosity of different compositions were evaluated. Microstructural studies such as aluminium-rich grain size, particle size and shape of ZrB_2 particles, their distribution in the matrix and presence of dislocations in matrix have also been evaluated and discussed in this chapter. Bulk hardness, ultimate tensile strength, and yield strength have been evaluated for all composites and finally contribution of different strengthening mechanisms in yield strength has been evaluated and discussed.

3.2 Differential Thermal Analysis (DTA)

DTA was conducted to study the endothermic and exothermic transformations with respect to the temperature during the composite preparation. When AA5052 alloy is

heated with two inorganic salts K_2ZrF_6 and KBF_4, several reactions take place in the following sequence as given below [Dinaharan et al., 2011],

$$K_2ZrF_6 + \frac{13}{3}Al = Al_3Zr + \frac{4}{3}AlF_3(g) + 2KF(g) \quad (3.1)$$

$$2KBF_4 + 3Al = AlB_2 + 2Al\,F_3(g) + 2KF(g) \quad (3.2)$$

$$Al_3Zr + AlB_2 = ZrB_2 + 4\,Al \quad (3.3)$$

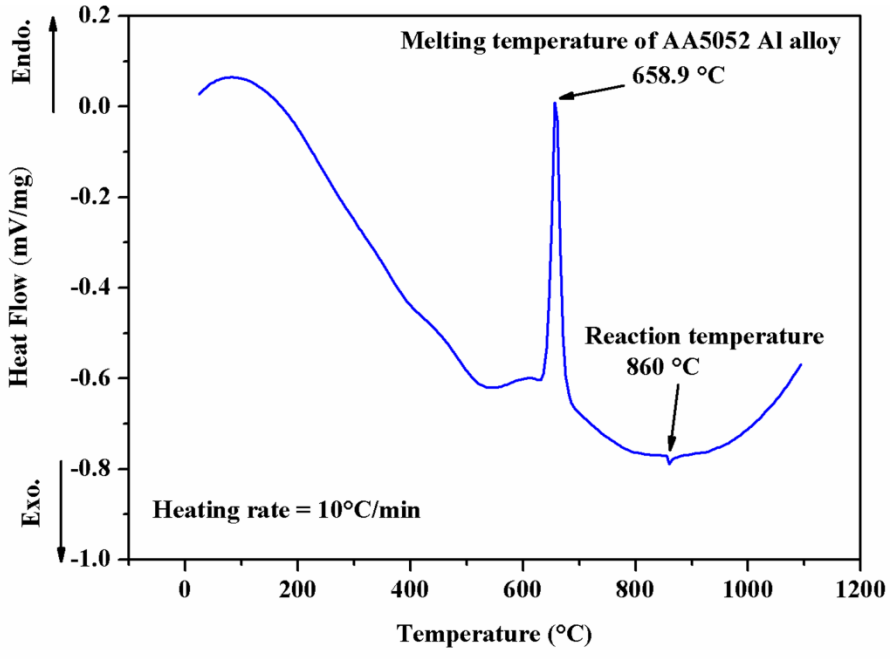

Figure 3.1 - DTA curve showing the endothermic and exothermic peaks during *insitu* reaction [Kumar et al., 2015b]

DTA curve shown in Fig. 3.1 consists of two peaks. First peak corresponds to endothermic reaction during melting of AA5052 alloy at 658.9°C, and the second peak corresponds to exothermic reaction (cf: eqn. 3.3) at 860°C, which indicates formation of ZrB_2 particles.

3.3 XRD Analysis and *insitu* Formation of ZrB_2 Particles

If the reaction time at 860°C is insufficient for the formation of ZrB_2 particles, it is more likely that Al_3Zr particles will be formed. Several trials were conducted to find the transformation time of 30 minutes. For all the compositions 30 minute of reaction time was given for complete transformation of Al_3Zr to ZrB_2. XRD analysis was conducted to verify the completion of reaction and the results are shown in Fig. 3.2a for AA5052/ZrB_2 composites with different compositions (i.e. 0, 3, 6, 9 and 10 vol. % of ZrB_2 particles). Diffraction peaks of ZrB_2 particles are clearly seen in all compositions confirming the presence of only ZrB_2 particles. It is also observed that intensity of the ZrB_2 diffraction peaks increases with increase in the vol. % of ZrB_2 particles. Peaks of intermetallic compounds Al_3Zr and AlB_2 are not observed which confirm completion of reaction (eqn. 3.3 of section 3.2). XRD pattern of extracted ZrB_2 particles is shown in Fig. 3.2b which further confirms the absence of any other intermetallic compound (AlF_3 and KF) in the composites which were in the gaseous form [Kumar et al., 2015b].

3.4 Density and Porosity Measurements

Density and porosity values of base alloy and composites are reported in Table 3.1. Experimental density of the base aluminium alloy and composites was calculated by Archimedes principle. Theoretical density was calculated by the rule of mixture. Density was observed to increase from 2.50 x 10^3 to 2.83 x 10^3 Kg/m^3 with increase in vol. % of ZrB_2 particles. Porosity in as-cast aluminium alloy AA5052 and composites was also calculated and it is within a limit of 4 to 7 vol. %.

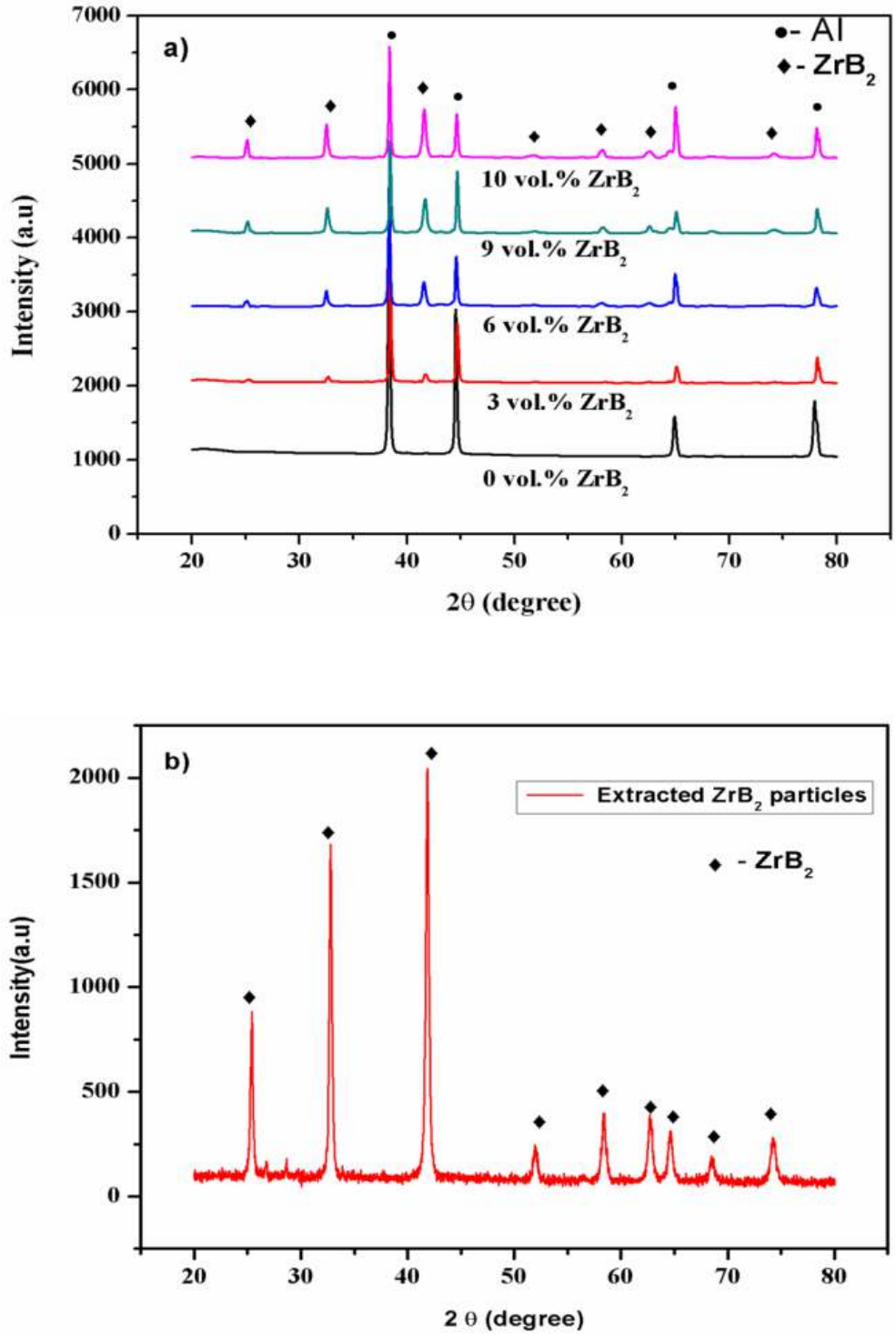

Figure 3.2 - XRD patterns of (a) AA5052/ZrB_2 composites and (b) extracted ZrB_2 particle for 9 vol. % composite[Kumar et al., 2015b]

Table 3.1- Average grain size, density and porosity of the base alloy and composites [Kumar et al., 2015b]

Material	Average grain size of Al-rich phase (μm)	Theoretical density ($\times 10^3$ Kg/m^3)	Experimental density ($\times 10^3$ Kg/m^3)	Porosity (vol. %)
AA5052 - 0 vol. % ZrB_2	115	2.68	2.50	6.7
AA5052 - 3 vol. % ZrB_2	101	2.78	2.66	4.3
AA5052 - 6 vol. % ZrB_2	84	2.88	2.73	5.2
AA5052 - 9 vol. % ZrB_2	67	2.98	2.80	6.0
AA5052 - 10 vol. % ZrB_2	55	3.02	2.83	6.3

3.5 Microstructural Examinations

3.5.1 Optical Microscopy

Figure 3.3a-e shows the optical micrographs of as cast base alloy and AA5052/ZrB_2 *insitu* composites with different vol. % of ZrB_2 particles. It is observed from the micrographs that *insitu* formed ZrB_2 particles appear in inter granular regions with some agglomeration or clustering. Grain refining tendency of ZrB_2 particles was observed from the microstructures. It is evident from the results that grain size of composites decreases with increase in the vol. % of ZrB_2 particles. Grain size distribution curves for different compositions are shown in Fig. 3.4a-e. Grain size of aluminium alloy matrix is reduced from 115 μm to 55 μm for composite having 10 vol. % ZrB_2 particles (Table 3.1). This reduction in grain size may be attributed to the restriction of growth of aluminium-rich grains due to the presence of ZrB_2 particles during solidification process. ZrB_2 particles act as a nucleus on which solidification of aluminium-rich grains takes place [Dinaharan et al., 2011]. With increasing vol. % of ZrB_2 more nucleation sites for aluminium-rich grains are created. Further, constitutional under cooling zone ahead of ZrB_2 particles also helps in refining the aluminium-rich grains. Thus, with the

increased number of ZrB_2 particles resistance is generated for the grain growth of aluminium matrix and it results in more refined grains of the matrix [Kumar et al., 2015b; 2015c; Rajan et al., 2013].

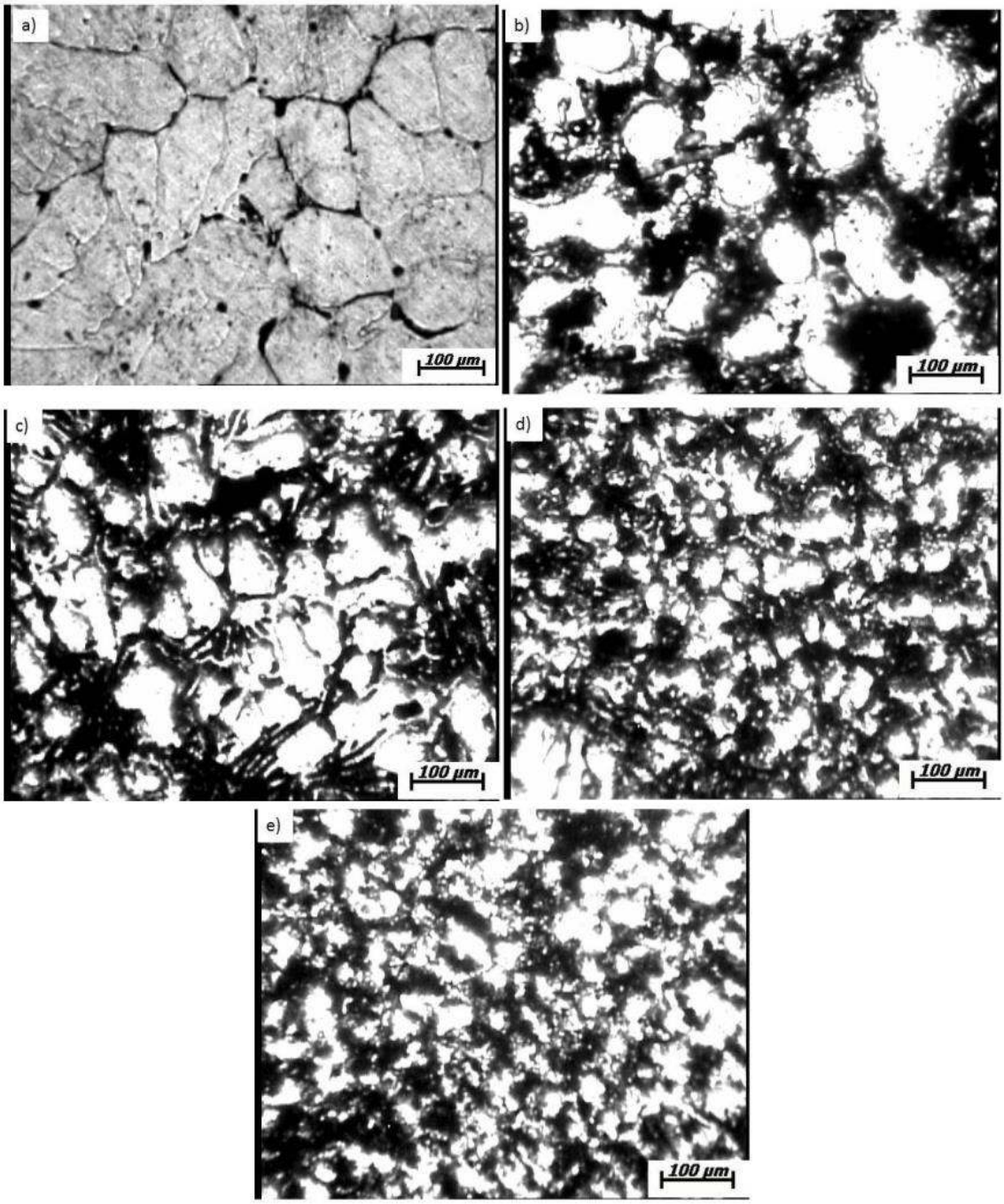

Figure 3.3 - Optical micrographs of (a) AA5052 - 0 vol. % ZrB_2 (b) AA5052 - 3 vol. % ZrB_2 (c) AA5052 - 6 vol. % ZrB_2 (d) AA5052 - 9 vol. % ZrB_2 and (e) AA5052 - 10 vol. % ZrB_2 [Kumar et al., 2015c]

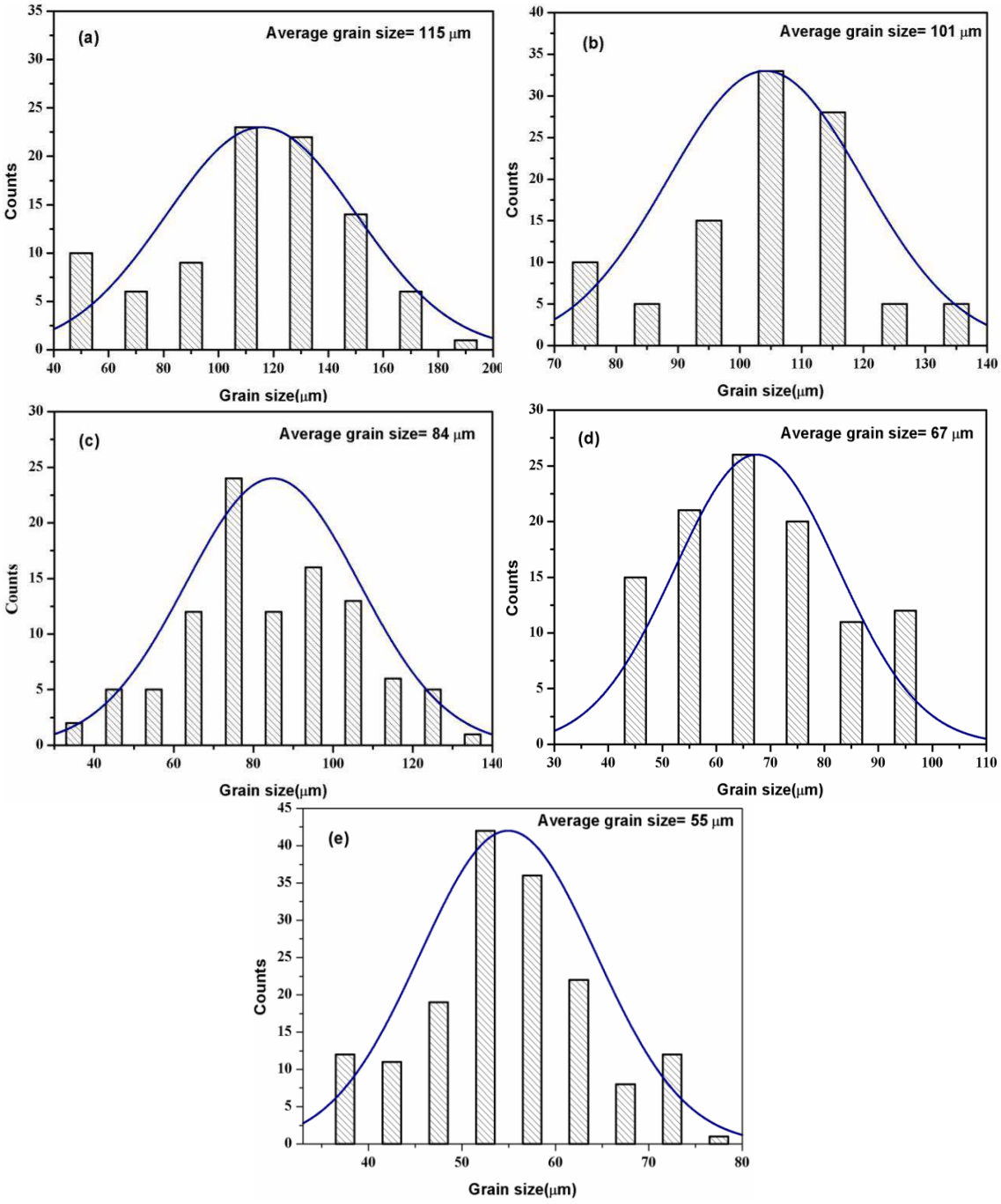

Figure 3.4 - Grain size distribution of (a) AA5052 - 0 vol. % ZrB_2 (b) AA5052 - 3 vol. % ZrB_2 (c) AA5052 - 6 vol. % ZrB_2 (d) AA5052 - 9 vol. % ZrB_2 and (e) AA5052 - 10 vol. % ZrB_2

3.5.2 SEM Examination

Figure 3.5a-d shows the SEM micrographs of composites containing different vol. % of ZrB_2 particles. Casting defects such as porosity, shrinkage, slag inclusion and cracks are not observed in the SEM micrographs which indicate the characteristics of sound

castings. It is observed that *insitu* formed ZrB_2 particles are uniformly distributed in the Al-rich matrix. However, agglomeration of the particles is also observed in few places and this phenomenon increases with increase in the amount of ZrB_2 particles. The distribution of ceramic particles in molten Al-rich matrix is significantly affected by the density difference between the matrix and ceramic particles during solidification. In the present work the density difference of matrix alloy and reinforced particles is more than $2g/cm^3$. As ZrB_2 particles are mostly in nanosize so these particles are likely to suspend for a long time in the melt which is an important condition for the uniform distribution of ZrB_2 particles [Han et al., 2002; Rajan et al., 2014]. In addition, wetting effect between reinforcement particles and molten aluminium matrix also restricts the movement of the ZrB_2 particles, thus, the particles can remain suspended for more time in the melt leading to uniform distribution [Dinaharan et al., 2011; Kumar et al., 2015b]. Morphology of ZrB_2 particles and corresponding EDS pattern are shown in Fig.3.5e-f.

3.5.3 TEM Examination

TEM study of the composites clearly reveals the morphology, interfacial characteristics, crystal structure and presence of dislocations in the matrix around ZrB_2 particles. Figure 3.6a-b shows the nanosize hexagonal and rectangular shape ZrB_2 particles at higher magnification. The difference in shape may be due to the breaking of columnar-like particles generated in the melt [Tian et al., 2014]. It is also evident from the figures that interface of matrix and ZrB_2 particle is clear and well bonded without any reaction product. It is reported that undesirable compounds may be present at the interface as a result of thermodynamic instability of ceramic particle in the aluminium melt [Davidson and Regener, 2000; Kumar and Murugan, 2012; Rajan et al., 2014]. Therefore, a clear interface is an essential requirement to enhance the load bearing capacity of PAMCs.

The clear interface and good bonding also retards the detachment of particles from the aluminium matrix. Hence, the hardness and strength of PAMCs are enhanced by ZrB_2 particles. Presence of clear interface may be attributed to thermodynamic stability of *insitu* formed ZrB_2 particles within melt which reduces the chance of oxidation of the particles, thus improving the interfacial bonding between matrix and particles. In addition, an increased local melt temperature, as a result of *insitu* reaction between salts and melt also improves the interfacial bonding [Lakshmi et al., 1998; Terry and Jones, 1990; Wood et al., 1993]. Most of the ZrB_2 particles are of nanometre size and few are of micron size. The particle size range is from 25 nm to 2 μm and the average size of ZrB_2 particle is 190 nm. Figure 3.6c-d shows the selected area diffraction (SAD) pattern corresponding to ZrB_2 particle and matrix. Indexing of diffraction pattern confirms Hexagonal Close Packed (HCP) and Face Centred Cubic (FCC) crystal structure of ZrB_2 particle and matrix respectively. It is reported that magnesium accelerates the nucleation rate of TiB_2 particles which promotes the formation of fine TiB_2 particles [Lohar et al., 2011]. In the present work magnesium present in the base alloy may also accelerate nucleation rate of ZrB_2 particles which leads to the formation of fine ZrB_2 particles. Dislocations in matrix along with ZrB_2 particles are also seen in Fig. 3.6e which contribute to hardness and strength of composites [Kumar et al., 2015b].

3.6 Mechanical Properties

The effect of ZrB_2 particles on mechanical properties like hardness, ultimate tensile strength (UTS), 0.2% yield strength (YS) and percentage elongation of the composites has been evaluated and presented in Table 3.2.

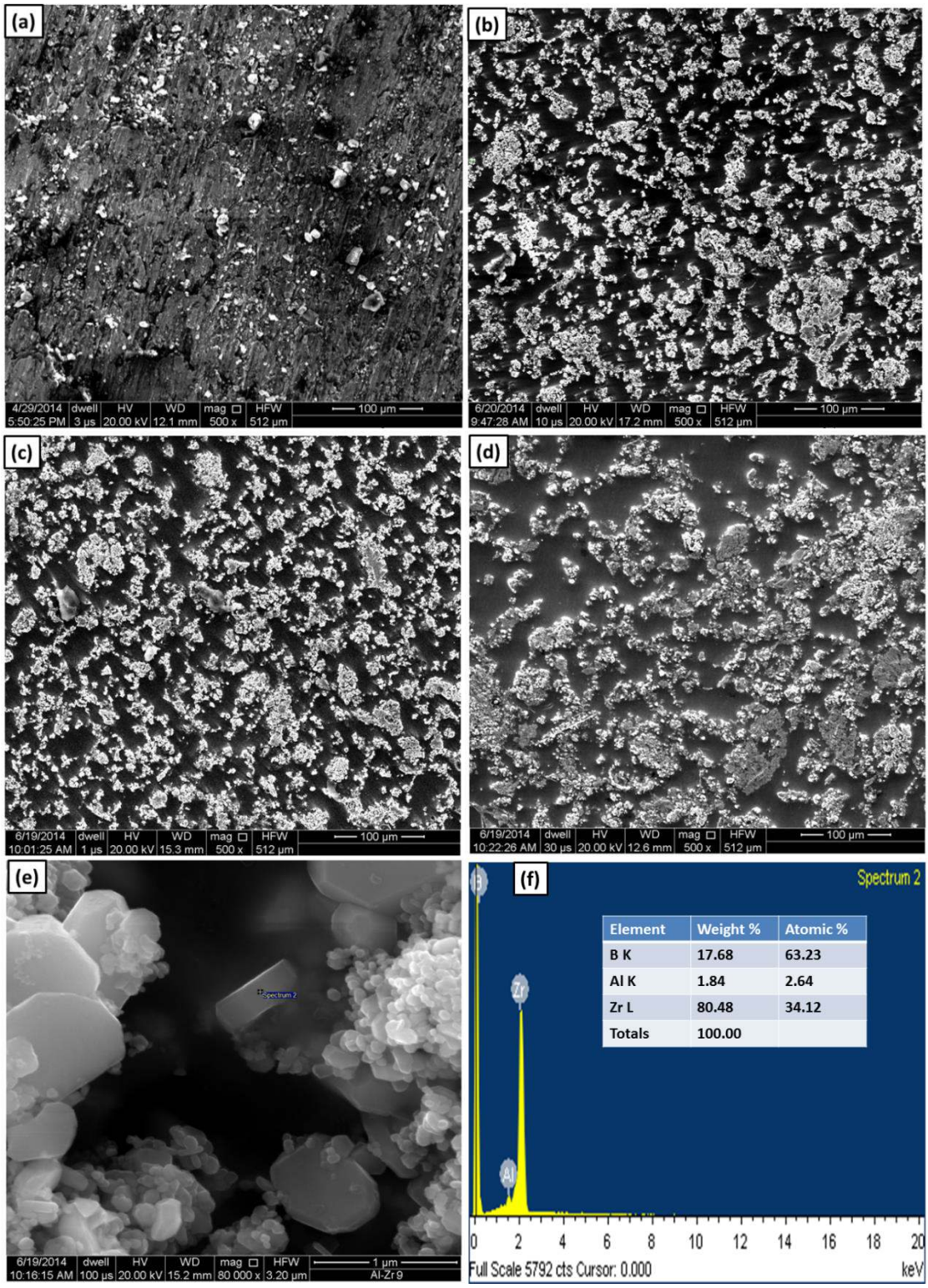

Figure 3.5 - SEM micrographs of (a) AA5052 - 3 vol. % ZrB_2 (b) AA5052 - 6 vol. % ZrB_2 (c) AA5052 – 9 vol. % ZrB_2 (d) AA5052 – 10 vol. % ZrB_2 (e) ZrB_2 at high magnification and (f) EDS pattern of ZrB_2 [Kumar et al., 2015b; 2015c]

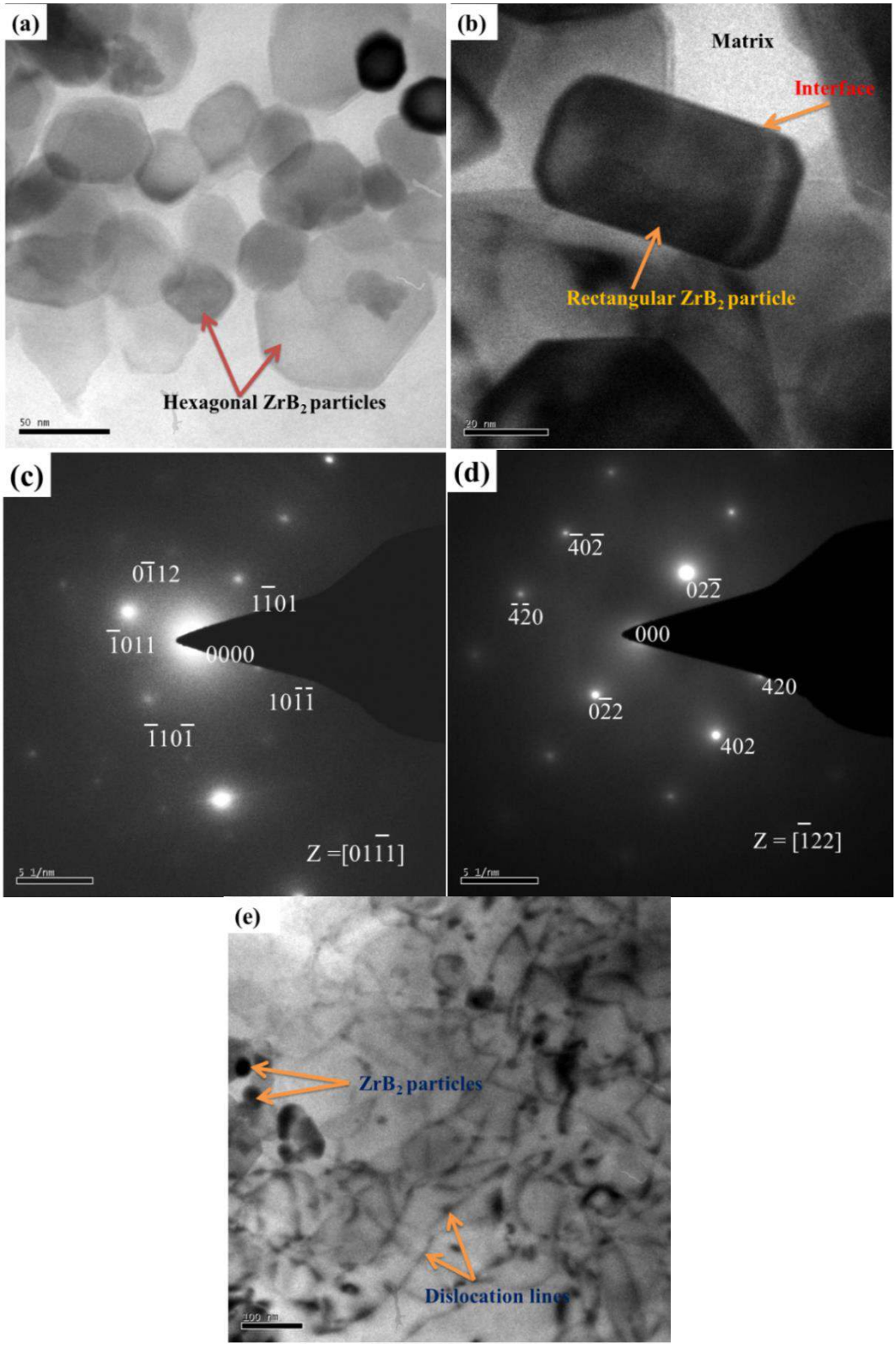

Figure 3.6 - TEM micrographs of (a-b) hexagonal and rectangular morphology of ZrB_2 (c) SAD pattern of ZrB_2 (d) SAD pattern of matrix and (e) dislocations present in the matrix [Kumar et al., 2015b; 2015c]

Table 3.2 - Mechanical properties of base alloy and composites [Kumar et al., 2015b]

Material	Hardness (BHN)	UTS (MPa)	0.2%YS (MPa)	% Elongation	n	K (MPa)
AA5052 - 0 vol. % ZrB_2	34 ± 1.58	89 ± 5.50	61 ± 4.04	6.23 ± 1.60	0.18115	176
AA5052 - 3 vol. % ZrB_2	38 ± 1.58	128 ± 1.00	70 ± 2.30	16.23 ± 0.96	0.18111	220
AA5052 - 6 vol. % ZrB_2	41 ± 1.32	153 ± 1.10	89 ± 4.50	14.30 ± 1.61	0.16258	254
AA5052 – 9 vol. % ZrB_2	48 ± 1.50	161 ± 6.80	112 ± 3.78	12 ± 3.02	0.14603	280
AA5052 - 10 vol. % ZrB_2	52 ± 0.86	142 ± 8.18	111 ± 8.62	7.7 ± 1.73	0.12477	248

3.6.1 Hardness

Figure 3.7 shows the variation of hardness (BHN) of base alloy and composites with vol. % of ZrB_2 particles. It is clearly observed that hardness increases with the increasing amount of ZrB_2 particles. The improvement in hardness may be attributed to the high dislocation density around the ZrB_2 particles due to difference in coefficient of thermal expansion (CTE) between Al-rich matrix and ZrB_2 particles [Dinaharan et al., 2011; Mandal et al., 2008]. Further, refinement of matrix phase and incorporation of hard ZrB_2 particles in the soft Al-rich matrix also contributes to the hardness. Better bonding between reinforcement and matrix and clear interface are also important factors which help to improve the hardness of the composites by increasing the load carrying capacity [Ramesh et al., 2010; 2011; Kumar et al., 2015b].

3.6.2 Tensile Properties

Tensile properties of base alloy and composites were evaluated at ambient temperature. UTS, 0.2% YS and percentage elongation have been evaluated from engineering stress-strain diagram. It is observed that UTS and yield strength of composites improve continuously up to 9 vol. % ZrB_2, but as the vol. % of ZrB_2 particles exceeds 9 vol. % both UTS and yield strength are adversely affected (Table 3.2). The variation of tensile

properties is shown in Fig.3.8. The reduction in strength may be attributed to generation of large number of reinforcement particles in the composite which results in large number of crack nucleation sites at particle matrix interface, therefore, early failure takes place [Mandal et al., 2008]. The decrease in strength beyond 9 vol. % may also be due to the agglomeration of ZrB_2 particles which may result in crack propagation and early interface debonding of ductile matrix during tensile deformation [Tian et al., 2014]. Composite with 9 vol. % ZrB_2 particles exhibits maximum values of UTS and yield strength which are improved by about 81 and 83% respectively as compared to base alloy. This improvement in strength may be attributed to grain refinement due to the presence of ZrB_2 particles, which is also in agreement with Hall-Petch relation. Increase in overall dislocation density around the ZrB_2 particles (Fig. 3.6e) due to mismatch of thermal expansion coefficients of aluminium matrix and ZrB_2 particles during solidification also contributes to strength [Khorramie et al., 2013; Yi et al., 2006b]. These *insitu* formed ZrB_2 particles restrict the motion of dislocations under load, and according to the Orowan strengthening mechanism the larger force is required for dislocations to overcome this resistance [Yoo et al., 2013; Zhang and Chen, 2008; Zhao et al., 2007]. Moreover, improvement may also result from solid solution strengthening. Efficient transfer of load from the matrix to the reinforcement particles and good interfacial bonding between matrix and particles are other contributing factors for increased strength [Kumar et al., 2015b; Lu et al., 2001; Ramesh et al., 2011; Zheng et al., 2014].

Ductility (% elongation) of composites is improved significantly as compared to base alloy (Table 3.2). During tensile deformation crack propagation is retarded by the fine *insitu* ZrB_2 particles. Presence of ZrB_2 particles can alter the direction of crack growth

which leads to the crack bridging, branching and deflection of crack from its favourable orientation with respect to the direction of applied load. More energy is utilized in these processes. Hence, resistance to crack propagation increases which leads to the improvement in fracture toughness and ductility of the composite is improved [Ramesh et al., 2011]. Further, the grain refinement also contributes to increased ductility as grain boundaries are more convoluted due to small grain size. These convoluted grain boundaries do not facilitate crack propagation. Thus, the fracture toughness of composites enhances leading to improved ductility. However, ductility of the composites decreases with increase in the vol. % of ZrB_2 particles (though still more than the base alloy). This may be due to the agglomeration of ZrB_2 particles at higher vol. % which leads to easy crack propagation and early failure of ductile matrix during tensile deformation [Tian et al., 2014; Kumar et al., 2015b].

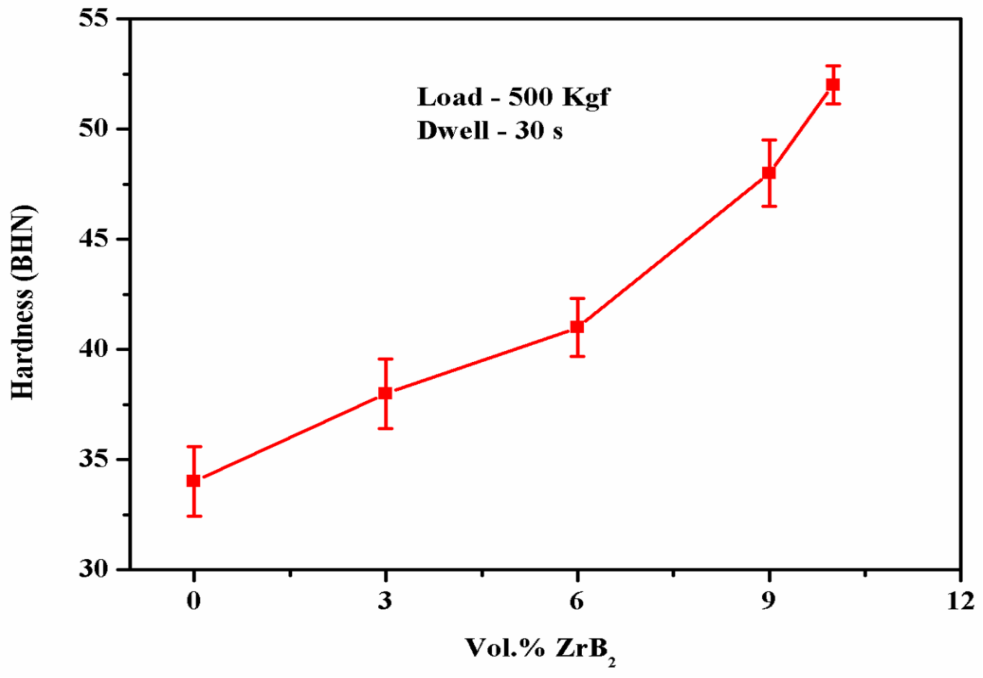

Figure 3.7 - Variation of hardness with vol. % of ZrB_2 particles in the composites [Kumar et al., 2015b]

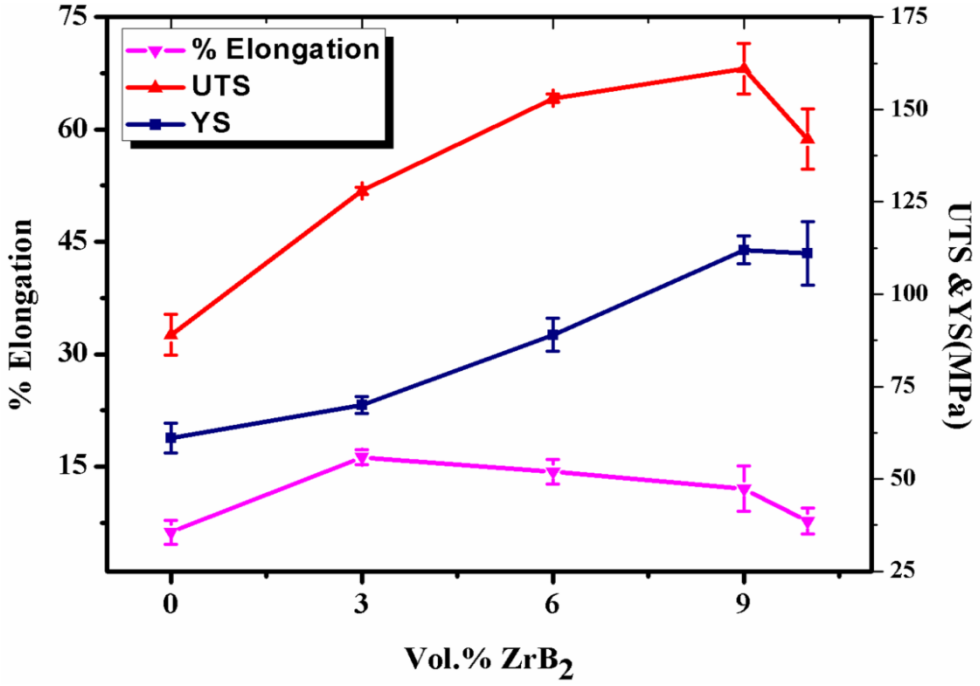

Figure 3.8 - Variation of tensile properties with vol. % ZrB_2 particles

Strain hardening behaviour of composites has also been studied by plotting the true stress (σ) against true plastic strain (ε_ρ) on log-log scale for base alloy and different composites (Fig. 3.9). The strain hardening exponent (n) and strength coefficient (K) calculated from equation $\sigma = K\varepsilon_p^n$ [Hollomon, 1945] represent the slope of the plots and intercept on y axis respectively at ε_ρ=1. It is observed that the value of n decreases as amount of ZrB_2 particles is increased, whereas, K increases with increasing amount of ZrB_2 (Table 3.2). Therefore, the composites with larger amount of ZrB_2 particles show higher strain hardening rate [Kumar et al., 2015b].

3.7 Fractography

Fractured surface was studied to identify the cause and type of failure in materials. Tensile fractured surfaces of base alloy and composites are shown in Fig. 3.10a-e. It is observed from Fig. 3.10a that fractured surface of base alloy has few small size dimples,

plane areas, cleavage fracture and shrinkage porosities which are indicative of brittle fracture. But all composites have mixed mode of fracture dominated by ductile nature (Fig. 3.10b-e). Composites have larger size dimples as compared to base alloy. But with increasing amount of ZrB_2 particles agglomeration takes place promoting crack initiation and propagation at the particle matrix interface which results into early failure. As a consequence, nature of fracture again shifts towards brittle side and ductility starts decreasing (Fig. 3.10b-e), but the ductility still remains higher than the base alloy (Table 3.2) [Kumar et al., 2015b].

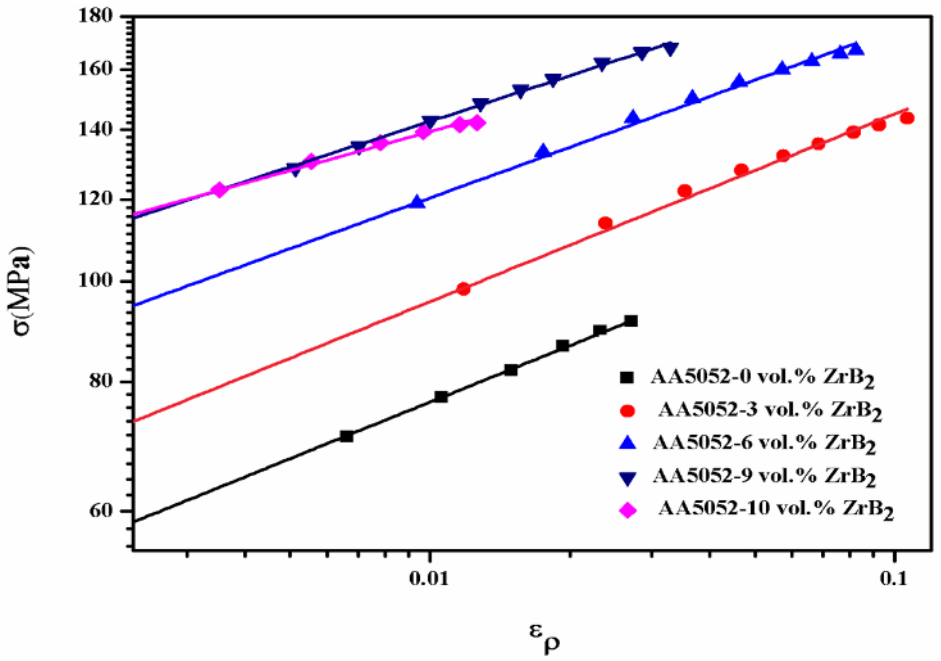

Figure 3.9 - σ vs. ε_ρ plot on log-log scale for composites [Kumar et al., 2015b]

3.8 Strengthening Mechanisms

Overall strengthening of AA5052/ZrB_2 composites is the combined contribution of different types of strengthening mechanisms such as Orowan strengthening, dislocation strengthening, grain-refined strengthening and solid solution strengthening.

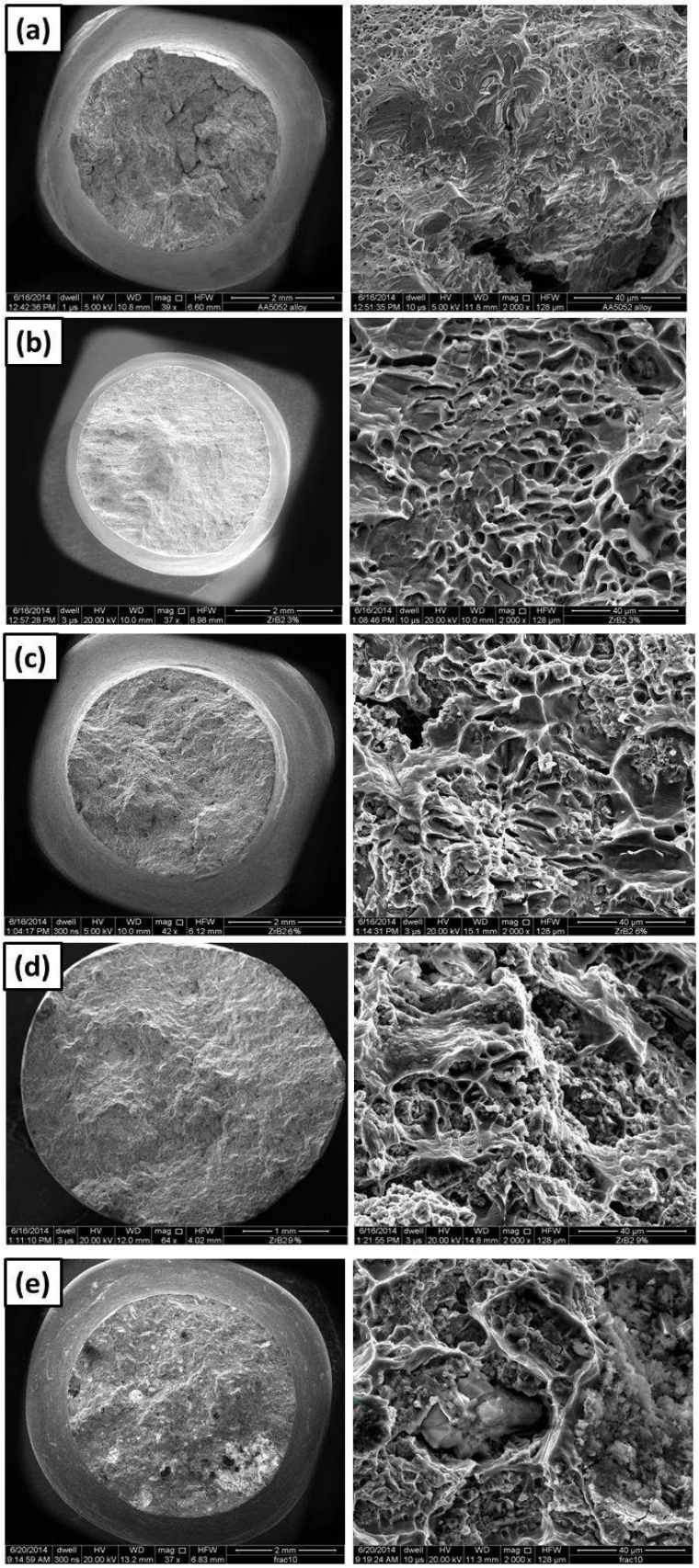

Figure 3.10 - Fractographs of (a) base alloy and composites with (b) 3 (c) 6 (d) 9 and (e) 10 vol. % ZrB_2 [Kumar et al., 2015b]

In order to develop the relationship between dislocations, grain size, particle size and their vol. % along with their solid solution strengthening effect, contribution of each strengthening mechanism to the yield strength of composites has been evaluated. The linear summation of each strengthening mechanism has been used to predict the yield strength of composites as given below in equation (3.4) [Zhao et al., 2008].

$$\sigma_{composite} = \Delta\sigma_{Orowan} + \Delta\sigma_{dislocation} + \Delta\sigma_{grain-refined} + \Delta\sigma_{solid-solution} \quad (3.4)$$

Different symbols and their values used for evaluating contribution of each strengthening mechanism are tabulated in Table 3.3.

Table 3.3 – Significance and values of symbols used in calculating strengthening mechanisms

Terms	Meaning	Values
G	Shear modulus of AA5052	25.9 GPa [Handbook, ASM, 1990b]
b	Magnitude of Burger's vector	$\sqrt{2}/_{2a}$= 0.286 nm, where, a (lattice constant) = 0.405 nm for FCC Al [Ma et al., 2014]
υ	Poisson ratio of AA5052	0.33 [Handbook, ASM, 1990b]
k_y	Hall-Petch coefficient	0.06 $MPam^{1/2}$ [Thangaraju et al., 2012]

3.8.1 Orowan Strengthening

Orowan strengthening in composites occurs due to interaction of dislocations with ZrB_2 particles which resists the propagation of cracks during loading. When composite bears a load, *insitu* formed ZrB_2 particles act as obstacles to hinder the motion of dislocations and strain field are created around ZrB_2 particles in the matrix. Resistance to propagation of cracks and dislocations motion increases with increase in vol. % of ZrB_2 particles which leads to enhanced strength of composite. The contribution of Orowan strengthening to yield strength of composite is calculated by following equation [Tong and Ghosh, 2001],

$$\Delta\sigma_{orowan} = \frac{2Gb}{2\pi\sqrt{(1-\upsilon)}}\frac{1}{\lambda_e}\ln(D/b) \quad (3.5)$$

Where, G is shear modulus of matrix alloy AA5052, b is the magnitude of Burger's vector, υ is the poisson's ratio of AA5052, D is the average diameter of ZrB_2 particle, and λ_e is the edge to edge particle spacing in the composites. λ_e is calculated as follows [Tong and Ghosh, 2001],

$$\lambda_e = D\sqrt{\left(\frac{\pi}{6V_f} - \frac{2}{3}\right)} \qquad (3.6)$$

Where V_f is the volume fraction of ZrB_2 particles in the composites. Value of λ_e has been calculated for 6 and 9 vol. % ZrB_2 composites with average ZrB_2 particle diameter D = 190 nm. Substituting the values of λ_e, G, b, υ and D in equation (3.5) from Table 3.3, contribution of Orowan strengthening has been calculated as $\Delta\sigma_{orowan} = 34$ and 42 MPa for 6 and 9 vol. % ZrB_2 composites respectively.

3.8.2 Dislocation Strengthening

Dislocations are generated in aluminium alloy matrix during solidification because of the mismatch in coefficient of thermal expansion (CTE) between matrix and ZrB_2 reinforcement particle. The dislocation density is the measure of number of dislocations present in unit volume.

Dislocation is a line defect and is defined as the total length of dislocation per unit volume. The higher dislocation density increases the strength of alloy. The amount of dislocations generation is affected by CTE, particle size, particle vol. % and matrix strength [Tong and Ghosh, 2001; Clyne and Withers, 1991].

In the present study dislocation density has been calculated by following formula [Zhao et al., 2004],

$$\rho = \frac{2\sqrt{2\varepsilon}}{db} \qquad (3.7)$$

Where, d and ε are crystallite size and lattice strain of composite, b is the Berger's vector and is defined as the $\sqrt{2}/2a$ in the term of lattice constant for FCC crystal structure. The value of Burger's vector b is calculated as 0.405 nm for FCC aluminium. Parameters d and ε are evaluated from Williamson-Hall equation [Williamson and Hall, 1953] as given below,

$$B\cos\theta_B = \frac{k_w\lambda}{d} + \varepsilon\sin\theta_B \qquad (3.8)$$

Where, B is the true peak broadening, λ is the wave length of CuKα incident radiation (λ = 1.5405 Å), k_w is about 0.9 and θ_B is the Bragg angle. The true peak broadening B, is calculated as,

$$B = \sqrt{B^2_{observed} - B^2_{instrument}} \qquad (3.9)$$

Where, $B_{observed}$ is the observed peak broadening in composites and $B_{instrument}$ is the instrumental broadening. XRD pattern of composite (Fig. 3.2a) has been used for calculating $B_{observed}$. After calculating the value of true peak broadening (B) from equation (3.9), liner fitted curve is drawn between B $\cos\theta_B$ and $\sin\theta_B$, and values of crystallite size (d) and lattice strain (ε) are given by slope and intercept of this fitted curve respectively.

If the values of b, d and ε are known the dislocation density of the composites can be calculated from equation (3.7), and for the present case values are 4.63×10^{14} and 5.21×10^{14} for 6 and 9 vol. % ZrB_2 composites respectively. These values will be further used in calculating the contribution to dislocation strengthening in the yield strength of composites. The dislocation strengthening contribution in yield strength of composites can be calculated by following equation [Aikin, 1997],

$$\Delta\sigma_{dislocation} = AGb\sqrt{\rho} \quad (3.10)$$

Where, A is the fractional surface area of ZrB_2 particles in the composites, G is the shear modulus of matrix, b is the Burger's vector and ρ is the dislocation density of the composites. Fractional surface areas calculated for 6 and 9 vol. % ZrB_2 composites are 0.171 and 0.175 respectively. The values of G and b are taken from Table 3.3, whereas, the dislocation density has been calculated using XRD analysis by equation (3.7). Thus, dislocation strengthening contribution can be calculated by substituting the values of G, A, b and ρ in equation (3.10) from Table 3.3, for 6 and 9 vol. % ZrB_2 composites. The values of $\Delta\sigma_{dislocation}$ are 27 and 30 MPa for composites with 6 and 9 vol. % ZrB_2 respectively.

3.8.3 Strengthening due to Grain Refinement

During grain refined strengthening, materials are strengthened by change in grain size. Strength increases with decrease in grain size. Grain boundaries act as obstacles to impede dislocation movement. Since, the grain lattice structure has different orientations, therefore, more energy is required for a dislocation to change direction and move into adjacent grain. Impediment to dislocation movement hinders the onset of plasticity which leads to increased yield strength of the material. In the present study ZrB_2 particles act as heterogeneous nucleation catalyst for aluminium. Moreover, ZrB_2 particles also act as obstacles and restrict the grain growth of aluminium during solidification resulting into more refined microstructure. Grain refined strengthening effect of ZrB_2 particles is increased with increase in volume fraction of ZrB_2 particles (Fig.3.3c-d). Contribution of this strengthening mechanism in composite's yield strength has been calculated by following equation (3.11) [Lloyd, 1994],

$$\Delta\sigma_{grain-refined} = k_y {d_g}^{-1/2} \quad (3.11)$$

Where, k_y is the Hall-Petch coefficient for matrix and d_g is the average grain size of aluminium grain in the composites.

The value of k_y has been taken from Table 3.3, while the grain size d_g has been calculated by an average of length and width of the aluminium grain in the composites. The grain size distribution of aluminium-rich grains in the composites are also shown in Fig. 3.4c-d with an average values of 84 μm and 67 μm for 6 and 9 vol. % ZrB_2 composites respectively. Substituting the values of k_y and d_g in equation (3.11) the grain-refined strengthening contribution is calculated. The values are $\Delta\sigma_{\text{grain-refined}}$ is 7 MPa for both the compositions.

3.8.4 Solid Solution Strengthening

In solid solution strengthening, strength of materials can be improved by alloying atoms of solute element into crystalline lattice of solvent element. When solute atoms are introduced into solvent, local stress fields are formed due to difference in their atomic size. These local stress fields interact with dislocations and impede their motion, causing an increase in yield strength of material. The contribution of solid-solution strengthening to yield strength in composites is calculated from the following equation (3.12) [Verhoeven, 1975],

$$\Delta\sigma_{\text{solid-solution}} = G\varepsilon\sqrt{x_f/4} \qquad (3.12)$$

Where, G is the shear modulus of matrix, ε is the fractional difference in zirconium and aluminium atomic diameters, and x_f is the fractional concentration of foreign atoms.

The ε has been calculated as 0.118. The calculated value of x_f is 0.055 and 0.081 for 6 and 9 vol. % ZrB_2 composites respectively. On substituting the values of G, ε and x_f in

equation (3.12) the solid-solution strengthening contribution has been calculated as 36 and 44 Mpa for composites with 6 and 9 vol. % ZrB_2 respectively.

The contribution of each strengthening mechanism has been given in Table 3.4. It is observed that the predicted yield strength of composites is slightly higher than the experimental values. Lesser experiment values of yield strength may be due to the clustering of ZrB_2 particles in the composites. Inter-particle bond in clusters is likely to be weak relative to those between ceramic and melt and intrinsic strength of the indivisible particles. This constitutes defects and lead to early failure.

Table 3.4 - Experimental yield strength and contribution of different strengthening mechanisms to yield strength of AA5052/ZrB_2 composites

Material	**Yield strength (MPa)**					
	Exp.	**Predicted**				
		$\Delta\sigma_{orowan}$	$\Delta\sigma_{dislocation}$	$\Delta\sigma_{grain-refined}$	$\Delta\sigma_{solid-solution}$	**Total**
AA5052 - 6 vol. % ZrB_2	89	34	27	7	36	104
AA5052 - 9 vol. % ZrB_2	112	42	30	7	44	123

3.9 Conclusions

Following conclusions are drawn -

1. AA5052/ZrB_2 composites containing different vol. % of ZrB_2 particles can be successfully produced by *insitu* reaction of molten aluminium alloy with two inorganic salts K_2ZrF_6 and KBF_4.
2. XRD spectrum of composites confirms the formation of ZrB_2 particles in aluminium matrix. Absence of any other compounds such as Al_3Zr and AlB_2

confirms the completion of *insitu* reaction. XRD of extracted particles provides secondary confirmation of the presence of only ZrB_2 particles in the composites.

3. DTA study confirms the reaction temperature (860°C) for synthesis of composite.
4. ZrB_2 particles work as a grain refiner and refine the grain size from 115 μm to 55 μm.
5. Microstructural examinations show uniform distribution of ZrB_2 particles in aluminium matrix. ZrB_2 particles are in hexagonal and rectangular shapes within a size range of 25 nm - 2 μm. Most of the ZrB_2 particles are in nanosize range.
6. Interface between the ZrB_2 particle and aluminium matrix was clear and well bonded.
7. There is significant improvement in mechanical properties due to *insitu* formation of ZrB_2 particles in composite.
8. Hardness continuously improved with increase in ZrB_2 content.
9. UTS, YS and % elongation show improvement up to 9 vol. % ZrB_2 composite and improved by 81, 83 and 93% respectively relative to base alloy, however, these parameters follow a decreasing trend beyond this composition.
10. Contribution of various strengthening mechanisms such as Orowan, dislocation, grain-refined and solid solution to yield strength of composites shows that there is good agreement between experimental and predicted values.
11. Orowan and solid solution strengthening are predominant mechanisms for improvement in strength of composites.

.